"Revision 1"

Phase diagram and P-V-T equation of state of Al-bearing seifertite at lowermost mantle conditions

D. Andrault [1], R.G. Trønnes [2], Z. Konôpková [3], W. Morgenroth [4], H.-P. Liermann [3], G. Morard [5] and M. Mezouar [6]

[1] Laboratoire Magmas et Volcans (LMV-OPGC), Université B. Pascal, Clermont-Ferrand, France

[2] Natural History Museum and Centre for Earth Evolution and Dynamics, University of Oslo, Norway

[3] Photone Sciences, Deutsches Elektronen-Synchrotron (DESY), Hamburg, Germany

[4] Institut für Geowissenschaften, Goethe University of Frankfurt, Germany

[5] Institut de Minéralogie, de Physique des Minéraux et de Cosmochimie (IMPMC), Paris, France.

[6] European Synchrotron Radiation Facility (ESRF), Grenoble, France

Abstract

We investigated the properties of Al-bearing SiO_2 (with 4 or 6 wt% Al_2O_3) at pressures and temperatures corresponding to the lowermost mantle, using laser-heated diamond anvil cell coupled with synchrotron-based in-situ X-ray diffraction. The phase transition from $CaCl_2$-structured to α-PbO_2-structured (seifertite) polymorphs occurs between 113 and 119 GPa at 2500 K. The range of pressure where the two phases coexist is small. There is a slight decrease of the transition pressure with increasing Al-content. We propose a tentative phase diagram reporting the minerals composition as a function of pressure in the SiO_2-Al_2O_3 system.

We also refine the P-V-T equation of state of Al-bearing seifertite based on volume

measurements up to more than 160 GPa and 4000 K (V_0= 92.73(10) Å^3, K_0= 304.2(3.0) GPa, K'_0=4.59 (fixed), Θ_{D0}=1130 K (fixed), γ_0=1.61 (3)). At 300 K, the volume decrease at the $CaCl_2$ to α-PbO_2 transition is 0.5(1) %, a value slightly lower than the 0.6% reported previously for Al-free samples. At high temperature, the Grüneisen parameter of seifertite is found to be similar to that of stishovite. Nevertheless, the $\Delta V/V$ across the $CaCl_2$-form to seifertite transition is found to increase slightly with increasing temperature.

Across the phase transition, volume changes can be translated into density changes only when the Al substitution mechanisms in both $CaCl_2$-form and seifertite are defined. The analysis of all available data sets suggests different substitution mechanisms for the two SiO_2 polymorphs. Al-substitution could occur via O-vacancies in the $CaCl_2$-form and via extra interstitial Al in seifertite. This would result in a density increase of 2.2(3) % at 300 K for SiO_2 in basaltic lithologies. Alternatively, the same Al-substitution mechanism in both of the SiO_2-dominated phases would yield a density increase of 0.5(1) %.

Keywords: Seifertite, phase transition in SiO_2, P-V-T equation of state, lowermost Earth mantle.

Introduction

Seismic tomography suggests that the slab behavior depends primarily on the original plate velocity, the penetration angle of the slab into the mantle and the age of the subducted crust. In several regions the slabs appear to flatten and be delayed near the 660 km discontinuity. In most regions, however, slabs eventually descend through the lower mantle (e.g. (van der Hilst et al., 2007; van der Meer et al., 2010)). The sinking of subducting slabs in the deep mantle is controlled primarily by the density difference between the slab materials and the ambient mantle, while the mantle viscosity governs the speed of the descent. Detailed tomographic mapping of high-velocity regions in the mantle and comparison with surface paleogeography indicate that most slab remnants

sink through the entire mantle in about 250 Ma, i.e. with an average speed of about 1.2 cm/year (van der Meer et al., 2010).

The slab density is partly related to the slab temperature but also to the intrinsic density of the various minerals and their relative proportions. Older and relatively colder slabs are expected to penetrate the deep mantle more easily. Still, a major complication is the layered structure of the subducted slab, including its sedimentary, basaltic and harzburgitic components. The density inversion between peridotite and basaltic material in the uppermost 50-100 km of the lower mantle caused by gradual transformation of majoritic garnet (e.g. (Ringwood, 1991)) led to the suggestion of partial segregation (flotation) of garnetite near the 660 km discontinuity. The low temperature and high viscosity of slab material, however, make such a lithological separation unlikely. Another possible site of basalt-peridotite separation is the core-mantle boundary (CMB) region. Sinking slab material deflected laterally along the CMB thermal boundary layer will be heated considerably, resulting in reduced viscosity (e.g. (Steinberger and Calderwood, 2006)). Even moderate basalt-peridotite density contrasts in the D" zone could therefore lead to such separation.

Difference in chemical composition between basaltic and peridotitic materials yields largely different mineral assemblages and mineral compositions at deep mantle P-T conditions. Peridotites varying from fertile lherzolite to depleted harzburgite are dominated by Mg-perovskite (pv, 70-80%) with minor amounts of ferropericlase (15-25%) and Ca-perovskite (Ca-pv, 0-10%). Basalts have 3-10 times higher concentrations of Al, Ti, Ca and Na and more than 5 times lower concentration of Mg than peridotite. The resulting lower mantle basaltic mineralogy has no ferropericlase and a low proportion of Mg-perovskite (or post-perovskite) with high Fe/Mg-ratio. Over-abundance of silica and alumina produces the separate silica-dominated (Irifune et al., 1994) and Al-rich phases (NAL and Ca-ferrite phases, (Akaogi et al., 1999; Miyajima et al., 1999)). At intermediate lower mantle depths, common basalts crystallize 15-20% $CaCl_2$-structured silica, 15-25% Ca-ferrite, 35-40% Mg-perovskite and 20-30% Ca-perovskite (Hirose et al., 1999). It is generally estimated that the Fe-rich Mg-perovskite makes basaltic material denser than peridotite

78 throughout the lower mantle below 720 km depth (e.g. (Guignot and Andrault, 2004; Hirose et al.,
79 2005; Ricolleau et al., 2010)). Partly due to its elevated bulk modulus, the $CaCl_2$-structured silica
80 phase becomes the least dense phase of the subducted slabs at 70-120 GPa, with a density
81 difference of more than 3 % relative to the most abundant Mg-rich silicate perovskite.

82 At ~2500 K, pure SiO_2 was reported to undergo a first-order phase transformation from the
83 $CaCl_2$-form to seifertite (adopting the α-PbO_2-structure (El Goresy et al., 2008)) at ~120 GPa, with
84 a dp/dT-slope of about 10 MPa/K (Murakami et al., 2003). In parallel, (Hirose et al., 2005) showed
85 that the silica-dominated phases in a basaltic composition display considerable Al_2O_3 solubility.
86 The presence of Al_2O_3 produces a considerable pressure reduction of the stishovite to $CaCl_2$-phase
87 transition, from ~50 GPa for pure SiO_2 to ~25 GPa for Al-bearing silica (Bolfan-Casanova et al.,
88 2009; Lakshtanov et al., 2007b). On the other hand, the effect of Al_2O_3 on the $CaCl_2$-form to
89 seifertite transformation and on the density change associated with this transition remains poorly
90 constrained. Our objective here is to further evaluate the phase and density relations in the binary
91 silica-alumina system at the P-T conditions of the lowermost mantle.
92
93 **Experimental methods**

94 Silica glasses with 4 and 6 wt% Al_2O_3 were prepared in Pt-crucibles at 1650-1670 °C in air,
95 using a vertical furnace at Centre for Material Science, University of Oslo and a Nabertherm
96 furnace at Bayerisches Geoinstitut, Bayreuth, Germany. Tiny air bubbles persisted even after 3-4
97 repetitions of re-grinding and re-melting. Electron probe microanalyses yield Al-contents of 4.1(4)
98 and 5.8(3) for glasses Al-4% and Al-6%, respectively. Relatively high values of standard deviations
99 denote persistence of some chemical heterogeneity in the glass. Our analytical precision yielded
100 element totals of 99.7(2) and 99.5(2) for more than 20 measurements on glasses Al-4% and Al-6%,
101 respectively. The glasses were finely powdered and mixed with 10-15 wt% Pt-powder which served
102 as a YAG laser absorber and a pressure indicator at high temperatures. Overall, our samples should
103 be homogeneous on a 2-3 micrometer scale, which corresponds to the size of our X-ray probe.

Pressures up to 120 GPa were generated by membrane-type diamond anvil cells (DAC) equipped with beveled diamonds of 150/300 or 100/300 µm diameters. Rhenium gaskets were pre-indented to ~25 µm thickness before laser drilling or spark erosion of 40-60 µm diameters holes. Sample pellets were loaded between two pieces of dry NaCl or KCl, which served as pressure transmitting medium and thermal insulator from the diamonds. Temperatures up to more than 4000 K were generated by two NIR Ytterbium fiber lasers. The size of the hot spot on the sample was kept between 15 and 25 µm by adjusting the distance between the focusing-lenses and the sample. Using the spectral radiometry method, precision in temperature determination is better than 50 K. This value is also a maximum for temperature fluctuations at high temperature. Because phase transformations between dense silica polymorphs are known to be sluggish and depend on the starting material and pressure–temperature history (Prakapenka et al., 2004), we heated for 20-40 min at each temperature point.

Pressures at 300 K were determined based on the equation of state (EoS) of platinum (Holmes et al., 1989). It enables quantitative comparisons with previous reports on the formation of seifertite (mostly (Hirose et al., 2005; Murakami et al., 2003)), in which Pt (Holmes et al., 1989) or Au (Tsuchiya, 2003) EoS were used. Pressures derived from Pt and Au were reported to be fully compatible between each other (Hirose et al., 2005). Alternatively, we used the NaCl-B2 EoS which has been calibrated against Pt (Sata et al., 2002). NaCl provides accurate pressure measurements after annealing at low temperature, when the Pt diffraction peaks remain broad due to poor release of the deviatoric stresses in the silica glass. At high temperature, the Pt that is intimately mixed with the starting material was used as a reliable sample-pressure indicator. We observe that the pressures measured at high temperatures are consistent with a pressure correction $\Delta P = 2.5\ 10^{-3}$ GPa/K (Andrault et al., 1998) compared to the nominal pressure measured at 300 K. The pressure error is estimated to be about 3%.

Angle dispersive X-ray diffraction was performed *in situ* at the P02.2 (PETRA III, DESY) and ID27 (ESRF) beamlines. We used a monochromatic X-ray beam tuned at 42.7 keV (P02.2) or 33

keV (ID27) focused to less than 2x2 μm^2 FWHM by two mirrors in the Kirkpatrick-Baez configuration. Diffraction images were acquired on a Perkin Elmer flat panel (P02.2) or Mar-CCD (ID27) detector with exposure times of 10-30 seconds, with or without sample rotation. Distance between sample and detector of 451 mm (P02.2) or 223 mm (ID27) was calibrated using a CeO_2 (P02.2) or LaB_6 (ID27) standard. Diffraction patterns were integrated and treated using the Fit2D (Hammersley, 1996) and the GSAS (Larson and Von Dreele, 1988) codes (Figures 1 and 2). The orthorhombic lattice (Pbcn) of seifertite contains 4 independent parameters for atomic positions plus thermal factors for Si and O atoms. Due to the limited number of crystallites present in the X-ray spot, we preferred to avoid refinement of all those parameters. We first performed full X-ray profile refinement, using the Rietveld mode and keeping all atomic positions fixed to the values previously reported in the literature (upper frames in Figure 2; (El Goresy et al., 2008)). Although the atomic parameters may evolve slightly with P and T, the changes will be minor because these parameters are closely linked to the atomic arrangement within the lattice. Consequently, the evolution of the diffraction peaks intensity with pressure should also be reduced. This technique allows to model the experimental peaks with d_{hkl} lines of comparable intensities and prevents evolution of the orthorhombic lattice toward solutions that are favorable from a mathematically rather than physical point of view. In a second step, we verified the adequateness between all experimental and theoretical diffraction features, using the Le Bail mode in which the peak intensities are adjustable parameters (lower frames in Figure 2; (Le Bail, 1992)). For the NaCl or KCl pressure medium and platinum, we adjusted each diffraction line intensity independently using the Le Bail method, in order to obtain a best refinement of the diffraction profile. More than 20 diffraction lines were used to identify the $CaCl_2$-structure and seifertite in two-theta ranges between 5 and 18 (P02.2) and 6 and 22 (ID27) degrees. The reduced chi-squared value are typically 0.15 or 0.07 for siefertite (or the $CaCl_2$-form) refined in Rietveld or Le Bail modes, respectively. The error in volume determination is less than 0.3%. The XRD data were acquired repeatedly during heating and after quenching to room temperature.

156

157 **Phase transformation from $CaCl_2$-form to seifertite**

158 We conducted 5 different runs (4 at P02.2 and 1 at ID27) of stepwise compression at 300 K
159 followed by laser heating at successively higher temperatures. When the same sample was used for
160 repeated experiments at increasing pressure, previously unheated sample areas were investigated at
161 each new pressure. Crystallization of the $CaCl_2$-form from the silica glass was obtained after laser
162 heating to 2500 K at 91, 98 and 106 GPa and at 90 and 107 GPa for the samples containing 4 and 6
163 wt% Al_2O_3, respectively. After further steps of incremental pressurization, heating led to the
164 formation of seifertite at nominal pressures of 119 and 121 GPa in the samples with 4 and 6 wt%
165 Al_2O_3, respectively. In the 5th experiment performed on the Al-6% glass at the ID27 beamline, we
166 observed pure $CaCl_2$-phase up to 108 GPa and 2500 K, a mixture of the two silica polymorphs
167 between 108 and 118 GPa, and pure seifertite starting from this pressure. Those results pinpoint at
168 ~2500 K the transition pressures at 108-119 GPa and 108-118 GPa for Al-4% and Al-6%
169 compositions, respectively. Those values are compatible with previous studies: At similar
170 temperatures, the transition pressure was reported at 122 GPa for pure SiO_2 (Murakami et al., 2003)
171 and between 100 and 113 GPa for MORB compositions (Hirose et al., 2005). Because our starting
172 material is a glass, we did not observe any metastable formation of seifertite at about 80 GPa as
173 reported previously from cristobalite starting material (Dubrovinsky et al., 2001; Shieh et al., 2005).
174 The glass crystallization is completed above ~3000K (Figures 1-3). In all cases, no further phase
175 transformation was observed upon heating after the glass crystallization. Although additional Al-
176 bearing phases were not detected, we cannot rule out Al_2O_3 saturation of the $CaCl_2$-structured and
177 seifertite phases. Such saturation would imply that the Al_2O_3-content in SiO_2-dominated phases are
178 lower than the 4 or 6 wt% of our starting materials. However, Al_2O_3 saturation in our seifertite is
179 unlikely, because seifertite crystallized from a natural basalt was previously reported with 12.8 wt%
180 Al_2O_3 (Hirose et al., 2005).

Based on the available data, we draw a tentative phase diagram for the Al-bearing SiO_2 compositions as a function of pressure (Figure 4). Due to the presence of Al-rich Ca-ferrite (near the $MgAl_2O_4$-$NaAlSiO_4$ join), the Al_2O_3 activity in a MORB composition is expected to be high but lower than unity. Therefore, the Al_2O_3-contents of 3.4 and 12.6 wt% of the $CaCl_2$-phase and seifertite, respectively, reported by Hirose et al. (2005), provide lower bounds for the Al_2O_3 solubility limit in silica. These values can hardly be used to calculate an Al partition coefficient between the two phases ($K_{Al}^{CaCl2/Seifertite}$), because the changes in mineralogy in their samples, between 60 GPa and 113 GPa, is likely to affect the Al-activity significantly. On the other hand, the pressure of 113 GPa for their run #6 corresponds to a higher bound for the $CaCl_2$-form to seifertite phase transition in case of saturation in Al_2O_3. The results for our two compositions provide constraints on the position of the phase loop between the two minerals. The binary phase loop tends towards lower pressure with increasing Al-content. We draw straight lines for phase boundaries compatible with all data sets in the phase diagram (Figure 4). By comparing the Al-contents in $CaCl_2$-phase and seifertite at a given pressure, we calculate a $K_{Al}^{CaCl2/Seifertite}$ value of ~0.55(5). For this value, the phase transformation for e.g. an Al-bearing silica composition with 5 wt% Al_2O_3 would extend from ~112 GPa to ~116 GPa, a pressure gap corresponding to a ~70 km thick transition interval at a depth of ~2500 km.

Results for the $CaCl_2$-form of silica

We report our SiO_2 volumes measured at 300 K for the $CaCl_2$-form below the transition pressure [Figure 5A]. We also report the data sets available for starting materials made of pure SiO_2 (Andrault et al., 2003; Murakami et al., 2003), MORB (Hirose et al., 2005), and an Al-bearing SiO_2 glass with 4 wt% Al_2O_3 (Bolfan-Casanova et al., 2009). In the latest study, stishovite was synthesized with an estimated Al_2O_3-content of 2.2-3.6 wt%, for a starting material containing 4 wt%. This range of values is comparable to 3.4 wt% Al_2O_3 measured in the $CaCl_2$-form by Hirose et al. (2005) and slightly less than the 4 and 6 wt% Al_2O_3 present in our starting materials. At this

point, it is interesting to note significant differences in the $CaCl_2$-form volumes between previous studies. The lowest compression curve, by ~1% of volume or 6 GPa compared to our previous studies, is that of pure SiO_2 reported by Murakami et al. (2003). At mid distance between those two curves plot the compression curve of MORB (Hirose et al., 2005). These differences could be due to a difference in pressure determination or in volume measurement of the silicate phase. Because no pressure medium was used in the previous studies, the most likely cause of experimental difference originates from pressure determination. The volume relaxation from high-temperature to 300 K for metallic blobs of Pt or Au pressure markers enclosed in a hard silica matrix can be hampered when shutting down the IR-laser. However, the volume change at the transition from $CaCl_2$-form to seifertite should be precise and significant for all studies, because the same experimental procedure was used throughout.

Our data set plots in perfect agreement with our prior studies performed on Al-free (Andrault et al., 2003) and 4 wt% Al_2O_3 (Bolfan-Casanova et al., 2009), irrespective of Al-composition. Using the same experimental methods, compression curves of the 4 starting materials (2 in previous studies and 2 in the present one) are found within the experimental error. It shows that Al presents a negligible effect on the volume of $CaCl_2$-structured silica at very high pressures. A study specifically dedicated to the effect of Al on the stishovite bulk modulus, using Brillouin scattering at ambient conditions, showed that addition of 6 wt% Al_2O_3 induces a ~8% decrease in bulk modulus K_0 (Lakshtanov et al., 2007a). However, the well-known tradeoff between K_0, its first pressure derivative K'_0, and maybe also second derivative K''_0, makes the compression curve very similar at high pressures. In our previous studies (dotted black line in Figure 5A), the Birch-Murnagham formalism was used to refine an isothermal (300 K) compression curve with the following parameters: $V_0 = 46.77$ Å^3, $K_0 = 292$ GPa and $K'_0 = 4.59$ (see sample PV-20 in Table 1 of (Bolfan-Casanova et al., 2009)), where V_0 is the unit cell volume at standard P-T conditions. In this study, we preferred the use of the Vinet EoS formalism for reference isotherms, in order to facilitate the comparison with a recent study on stishovite (Wang et al., 2012). We therefore adjusted the

previous compression curve using the Vinet EoS and obtained V_0 = 46.77 Å^3 (fixed), K_0 = 297(7) GPa and K'_0 = 4.59 (fixed).

To our knowledge, there is no study reporting the EoS of the $CaCl_2$-form of Al-bearing SiO_2 phases at high pressures and temperatures. A previous work performed up to 54 GPa and 1700K reports the following parameters for the high temperature properties of stishovite: Θ_{D0}=1130 K, γ_0=1.67, a=1, b=3, where Θ_{D0} and γ_0 are the Debye temperature and the Grüneisen parameter at standard P-T conditions, respectively (Wang et al., 2012). The EoS formalism was based on Mie-Grüneisen-Debye to model the high temperature properties. In absence of a more reliable data set, we assume the following parameters to estimate volumes of the $CaCl_2$-form at all P-T conditions: V_0= 46.77 Å^3, K_0= 297 GPa, K'_0= 4.59, Θ_{D0}=1130 K, γ_0=1.67, a=1, and b=3. Based on this PVT EoS, we calculate volumes of the $CaCl_2$-form at 300, 2000 and 4000 K in the pressure range investigated in this study (Figure 5B).

P-V-T equation of state of seifertite

We also report our SiO_2 volumes measured at 300 K [Figure 5A] and at temperatures up to 4300 K [Figure 5B] for seifertite between the transition pressure and 162 GPa. Because seifertite and the $CaCl_2$-structured phase have 4 and 2 formula units per unit cell, respectively, we divide the seifertite volume by 2 to simplify the comparison. As for the $CaCl_2$-form, we also report data sets for pure SiO_2 (Murakami et al., 2003) and MORB (Hirose et al., 2005). We first refine the P-V-300K EoS of seifertite of Al-6 composition to V_0= 92.73(10) Å^3, K_0= 304.2(3.0) GPa and K'_0=4.59 (fixed), using the 14 data points recorded at ambient temperature in this study [Table 1]. We fix K'_0 because our experimental data set does not allow to adjust precisely the 3 parameters independently, due to the dependency between K_0 and K'_0 values. The seifertite bulk modulus appears very similar to that of the $CaCl_2$-form, only ~2% higher than the value of 297 GPa recalculated for K'_0 = 4.59, based on a study using precisely the same experimental methods (Bolfan-Casanova et al., 2009). If we fix K'_0=5.0, we obtain V_0= 93.75(10) Å^3 and K_0= 270.3(3.0) GPa. The bulk modulus is found

~7% lower than the 292 GPa reported for stishovite in a previous study using a large volume press apparatus (Wang et al., 2012).

At high temperature, we refine Θ_{D0}=1130 K (fixed), γ_0=1.61(3), a=1 (fixed) and b=3 (fixed) [Table 2], using the 16 data points recorded in this study [Table 1]. The choice of fixing Θ_{D0}, a, and b is to facilitate the quantitative comparison with a previous study on stishovite (Wang et al., 2012). With these parameters, the maximum difference between the experimental and theoretical pressures is 2.7 GPa, which is within the experimental uncertainties. The refined room pressure Grüneisen parameter of seifertite appears very similar to that proposed recently for stishovite, which was reported as 1.67 (Wang et al., 2012). In the P-T range investigated, we calculate Debye temperature and Grüneisen parameter mean values of Θ_D=1488(20) K and γ=0.78(4), respectively (the Θ_{D0} and γ_0 reported above are ambient values). Based on this PVT EoS, we calculate volumes of seifertite at 300, 2000 and 4000 K for the pressure range investigated in this study (Figure 5B).

We finally analyzed the evolution of the seifertite cell parameters with pressure (Figure 6). We treated the fictive volumes a^3, b^3 and c^3 in a similar manner like seifertite unit cell volumes. It results in a set of isothermal and high temperature elastic parameters [Table 2]. The Seifertite unit cell is quite anisotropic at high P and T, with the a parameter being 30% less incompressible than b and c, and with the b parameter showing a Grüneisen parameter about twice of a and c.

Density change across the phase transition

A comparison between the 300 K isothermal compression curves of the $CaCl_2$-form and seifertite of Al-6 composition evidences a volume change $\Delta V/V$= -0.5(1)% across the phase transition [Figure 5A]. This value is very comparable to the volume changes of -0.6% refined for pure SiO_2 (Murakami et al., 2003). For temperatures of 2000 and 4000 K, we refine volume changes of -0.52(10) % and -0.62(10) %, respectively, based on the PVT EoS [Figure 5B]. The fact that $\Delta V/V$ increases slightly with temperature is compatible with a Grüneisen parameter lower in seifertite compared to the $CaCl_2$-form.

The volume reduction of -0.6% observed for pure SiO_2 (Murakami et al., 2003) translates directly in a +0.6% density change at the transition. However, the relationship between volume and density is more complex for Al-bearing SiO_2 compounds. Three different mechanisms are possible for the Al_2O_3 insertion in SiO_2 (Bromiley et al., 2006; Hirose et al., 1999): (a) Formation of one oxygen vacancy per two Si^{4+} substituted by Al^{3+}; (b) Addition of one extra-interstitial Al^{3+} (i.e. a total of four Al^{3+}) when three Si^{4+} are replaced; (c) A coupled (Al^{3+},H^{+}) substitution in the presence of hydrogen. Also, one should keep in mind that different substitution mechanisms could still coexist in the same silica phase. Deriving density changes from volume changes at the phase transition requires assumptions on the predominant Al substitution mechanism in both the low and high pressure forms of SiO_2. The reason is that the number of atoms per unit cell, and thus the corresponding atomic mass, is not the same for the three different Al-substitution mechanisms. Based on volume variations available for various Al-bearing compositions, we calculate density changes that should be expected at the transition for all possible types of substitution mechanisms in $CaCl_2$-form and seifertite (Table 3).

Thermodynamic principles require a density increase (a positive $\Delta\rho$) for the pressure-induced phase transformation irrespective of composition. Therefore, some Al-substitution mechanisms can be readily eliminated. First of all, having an identical substitution mechanism (ISM) for both polymorphs would yield a 2.3% density reduction at the transition pressure for Al-bearing silica in the MORB material (Hirose et al., 2005). This situation is not impossible, because this negative $\Delta\rho$ could be counterbalanced by complementary mineralogical changes and element partitioning in the multi-component material. However, a largely negative $\Delta\rho$ would be surprising and we therefore search for a more likely situation. The O-vacancy substitution mechanism in seifertite is unlikely, because this would cause negative $\Delta\rho$ in our samples whatever is the Al_2O_3-substitution mechanisms in the $CaCl_2$-form (once the ISM case is discarded). In the same way, the Al-interstitial mechanism is unlikely in the $CaCl_2$-form. In a study at pressures up to 25 GPa, it was shown that the mechanism involving coupled Al^{3+} and H^{+} substitution can only explain 40% of the Al-

311 substitution in stishovite (Litasov et al., 2007). In our experiments, particular care was taken to
312 prevent the presence of water. Also, any water present in one polymorph is also likely to be present
313 in the other, which would yield a similar Al-substitution mechanism in both polymorphs (the ISM
314 case).

315 The most likely mechanisms are therefore the O-vacancy substitution in the $CaCl_2$-form and the
316 Al^{3+}-interstitial substitution in seifertite (the O->Al mechanism in Table 3). This is the only
317 scenario in which the phase transition obeys the thermodynamic rule of density increase for all the
318 data sets available. It is compatible with a previous study showing that formation of O-vacancies is
319 the predominant mechanism for the Al-substitution in stishovite (Bromiley et al., 2006). It remains
320 unknown how it evolves with the increasing pressure in the rutile-structure, as well as across the
321 structural distortion that yields the $CaCl_2$-type structure. For our samples with 4 or 6 wt% Al_2O_3,
322 the O->Al mechanism would imply a ~2.19% density increase at the phase transition. This density
323 increase is significantly larger than for the pure SiO_2 system ($\Delta\rho/\rho$~0.6%), in agreement with a
324 lowering of the transition pressure with increasing the Al-content. In MORB, the density change is
325 smaller, with a value of ~0.23%, because of the strong Al-partitioning into seifertite.

326

327 **Buoyancy of the subducted slabs**

328 Recent studies agree that basaltic materials of subducted slabs have a slight, but significant,
329 density excess compared to a peridotitic lower mantle, even if the slabs are thermally equilibrated.
330 Depending on composition and pressure, a density difference of 0.4 to 4.0 wt% was reported
331 (Guignot and Andrault, 2004; Hirose et al., 2005; Ono et al., 2005; Ricolleau et al., 2010). MORBs
332 with elevated Fe-content are clearly denser. Despite the density excess, basaltic material under
333 lower mantle conditions contains free silica phases, which are the lowest density phases at depths
334 exceeding 1600-1800 km. Altogether, some studies suggest a decrease of the MORB density excess
335 with increasing mantle depth (Guignot and Andrault, 2004; Ricolleau et al., 2010) and others
336 suggest a constant $\Delta\rho$ (Hirose et al., 2005; Ono et al., 2005). For sedimentary material, the density

is significantly lower than for MORB, due to low Fe and high Si-contents (Guignot and Andrault, 2004).

Our experimental results on compositions with 4-6 wt% Al_2O_3 suggest a ~2.19 % density increase for the transition from the $CaCl_2$-structured form to seifertite at 113-119 GPa and 300 K. At temperatures above 2000 K, this value should reach ~3%, due to higher volume change found for this transition at high temperature. The strong Al-partitioning from the $CaCl_2$-structured phase into seifertite will lead to compositional and density adjustments of the other Al-bearing phases in basaltic lithologies, in addition to the density effects caused by the silica-dominated phase transition. In subducted slab material the silica-dominated phases can represent up to about 20 and 40 vol% of MORB and sedimentary components, respectively (Hirose et al., 1999; Irifune et al., 1994). The $CaCl_2$-structured phase to seifertite transition could have a minor effect on the buoyancy in the peridotitic mantle of the basaltic ocean crust of subducted slabs, because free-SiO_2 is not highly abundant and the MORB density is already significantly higher. For the sedimentary component, however, the $CaCl_2$ to seifertite transition may have a larger impact and facilitate the descent of the sedimentary material to the lowermost part of the mantle.

Acknowledgements

X-ray measurements were carried out at the light source PETRA III at DESY, a member of the Helmholtz Association (HGF), and at the ESRF. Experimental costs for the high-pressure experiments were defrayed by a Småforsk grant from the Research Council of Norway and the Programme National de Planétologie (INSU-CNRS). RGT, and WM are supported by CoE-grant 223272 (CEED) from RCN, and BMBF projects number 05K10RFA and 05K13RF1, respectively. We thank the Am. Min. editors O. Tschauner and K. Putirka for their constructive work to improve this paper. This is a Clervolc contribution n°XXX.

References cited:

Akaogi, M., Hamada, Y., Suzuki, T., Kobayashi, M., and Okada, M. (1999) High pressure transitions in the system MgAl2O4-CaAl2O4: a new hexagonal aluminous phase with implication for the lower mantle. Physics of the Earth and Planetary Interiors, 115, 67-77.

Andrault, D., Angel, R.J., Mosenfelder, J.L., and Le Bihan, T. (2003) Equation of state of the stishovite to lower mantle pressures. American Mineralogist, 88, 301-307.

Andrault, D., Fiquet, G., Itié, J.P., Richet, P., Gillet, P., Häusermann, D., and Hanfland, M. (1998) Thermal pressure in a laser-heated diamond-anvil cell: An x-ray diffraction study. European Journal of Mineralogy, 10, 931-940.

Bolfan-Casanova, N., Andrault, D., Amiguet, E., and Guignot, N. (2009) Equation of state and $CaCl_2$ transformation of Al-bearing stishovite up to 100 GPa and 3000 K. Physics of the Earth and Planetary Interior, 174(1-2), 70-77.

Bromiley, G.D., Bromiley, F.A., and Bromiley, D.W. (2006) On the mechanisms for H and Al incorporation in stishovite. Physics and Chemistry of Minerals, 33(8-9), 613-621.

Dubrovinsky, L.S., Dubrovinskaia, N.A., Saxena, S.K., Tutti, F., Rekhi, S., Le Bihan, T., Shen, G.Y., and Hu, J. (2001) Pressure-induced transformations of cristobalite. Chemical Physics Letters, 333(3-4), 264-270.

El Goresy, A., Dera, P., Sharp, T.G., Prewitt, C.T., Chen, M., Dubrovinsky, L., Wopenka, B., Boctor, N.Z., and Hemley, R.J. (2008) Seifertite, a dense orthorhombic polymorph of silica from the Martian meteorites Shergotty and Zagami. European Journal of Mineralogy, 20(4), 523-528.

Guignot, N., and Andrault, D. (2004) Equations of state of Na-K-Al host phases in the lower mantle and implications for MORB density in the lower mantle. Physics of the Earth and Planetary Interiors, 134-144, 107-128.

Hammersley, J. (1996) Fit2d user manual. ESRF, Grenoble, France.

Hirose, K., Fei, Y.W., Ma, Y.Z., and Mao, H.K. (1999) The fate of subducted basaltic crust in the Earth's lower mantle. Nature, 397(6714), 53-56.

Hirose, K., Takafuji, N., Sata, N., and Ohishi, Y. (2005) Phase transition and density of subducted MORB crust in the lower mantle. Earth and Planetary Science Letters, 237(1-2), 239-251.

Holmes, N.C., Moriarty, J.A., Gathers, G.R., and Nellis, W.J. (1989) Equations of state of platinum to 660 GPa (6.6 Mbar). Journal of Applied Physics, 66, 2962-2967.

Irifune, T., Ringwood, A.E., and Hibberson, W.O. (1994) Subduction of continental crust and terrigenous and pelagic sediments: an experimental study. Earth and Planetary Science Letters, 126, 351-368.

Lakshtanov, D.L., Litasov, K.D., Sinogeikin, S.V., Hellwig, H., Li, J., Ohtani, E., and Bass, J.D. (2007a) Effect of Al3+ and H+ on the elastic properties of stishovite. American Mineralogist, 92(7), 1026-1030.

Lakshtanov, D.L., Sinogeikin, S.V., Litasov, K.D., Prakapenka, V.B., Hellwig, H., Wang, J.Y., Sanches-Valle, C., Perrillat, J.P., Chen, B., Somayazulu, M., Li, J., Ohtani, E., and Bass, J.D. (2007b) The post-stishovite phase transition in hydrous alumina-bearing SiO2 in the lower mantle of the earth. Proceedings of the National Academy of Sciences of the United States of America, 104(34), 13588-13590.

Larson, A.C., and Von Dreele, R.B. (1988) GSAS Manual. Report LAUR 86-748. Los Alamos National Laboratory.

Le Bail, A. (1992) Extracting structure factors from powder diffraction data by iterating full pattern profile fitting. In E. Prince, and J.K. Stalick, Eds. Accuracy in Powder Diffraction, p. 213. National Institut of Standard and Technology.

Litasov, K.D., Kagi, H., Shatskly, A., Ohtani, E., Lakshtanov, D.L., Bass, J.D., and Ito, E. (2007) High hydrogen solubility in Al-rich stishovite and water transport in the lower mantle. Earth and Planetary Science Letters, 262(3-4), 620-634.

Miyajima, N., Fujino, K., Funamori, N., Kondo, T., and Yagi, T. (1999) Garnet-perovskite transformation under conditions of the Earth's lower mantle: an analytical transmission electron microscopy study. Physics of the Earth and Planetary Interiors, 116, 117-131.

Murakami, M., Hirose, K., Ono, S., and Ohishi, Y. (2003) Stability of CaCl2-type and alpha-PbO2-type SiO2 at high pressure and temperature determined by in-situ X-ray measurements. Geophysical Research Letters, 30(5).

Ono, S., Ohishi, Y., Isshiki, M., and Watanuki, T. (2005) In situ X-ray observations of phase assemblages in peridotite and basalt compositions at lower mantle conditions: Implications for density of subducted oceanic plate. Journal of Geophysical Research-Solid Earth, 110(B2).

Prakapenka, V.P., Shen, G.Y., Dubrovinsky, L.S., Rivers, M.L., and Sutton, S.R. (2004) High pressure induced phase transformation of SiO2 and GeO2: difference and similarity. Journal of Physics and Chemistry of Solids, 65(8-9), 1537-1545.

Ricolleau, A., Perrillat, J.-P., Fiquet, G., Daniel, I., Matas, J., Addad, A., Menguy, N., Cardon, H., Mezouar, M., and Guignot, N. (2010) Phase relations and equation of state of a natural MORB: Implications for the density profile of subducted oceanic crust in the Earth's lower mantle. Journal of Geophysical Research-Solid Earth, 115, B08202.

Ringwood, A.E. (1991) Phase-transformations and their bearing on the constitution and dynamics of the mantle. Geochimica et Cosmochimica Acta, 55(8), 2083-2110.

Sata, N., Shen, G., Rivers, M.L., and Sutton, S.R. (2002) Pressure-volume equation of state of the high-pressure B2 phase of NaCl. Physical Review B, 65, 114114-7.

Shieh, S.R., Duffy, T.S., and Shen, G.Y. (2005) X-ray diffraction study of phase stability in SiO_2 at deep mantle conditions. Earth and Planetary Science Letters, 235(1-2), 273-282.

Steinberger, B., and Calderwood, A.R. (2006) Models of large-scale viscous flow in the Earth's mantle with constraints from mineral physics and surface observations. Geophysical Journal International, 167(3), 1461-1481.

Tsuchiya, T. (2003) First-principles prediction of the P-V-T equation of state of gold and the 660-km discontinuity in Earth's mantle. Journal of Geophysical Research-Solid Earth, 108(B10).

van der Hilst, R.D., de Hoop, M.V., Wang, P., Shim, S.H., Ma, P., and Tenorio, L. (2007) Seismostratigraphy and Thermal Structure of Earth's Core-Mantle Boundary Region. Science, 315(5820), 1813 - 1817.

van der Meer, D.G., Spakman, W., van Hinsbergen, D.J.J., Amaru, M.L., and Torsvik, T.H. (2010) Towards absolute plate motions constrained by lower-mantle slab remnants. Nature Geoscience, 3(1), 36-40.

Wang, F.L., Tange, Y., Irifune, T., and Funakoshi, K. (2012) P-V-T equation of state of stishovite up to mid-lower mantle conditions. Journal of Geophysical Research-Solid Earth, 117, B06209.

Table 1: Unit cell parameters of seifertite of 6 wt% composition recorded from 100 to 162 GPa and 300 to 4300 K. Pressure is derived from the PVT-EoS of platinum (Holmes et al., 1989) and temperature was determined by radiometric measurements. Uncertainties are 3% for pressures, 50 K for high temperatures, ~0.005 Å for (a, b, c) cell parameters and ~0.1 $Å^3$ for unit cell volumes.

		Seifertite				
T [K]	**P [K]**	**A [Å]**	**B [Å]**	**C [Å]**	**V [$Å^3$]**	**V/2 [$Å^3$]**
300	102.4	3.785	4.722	4.201	75.10	37.55
3410	117.8	3.778	4.736	4.197	75.10	37.55
300	105.7	3.767	4.723	4.198	74.69	37.35
3400	121.2	3.779	4.717	4.190	74.69	37.35
3200	121.0	3.768	4.718	4.191	74.50	37.25
300	118.9	3.755	4.676	4.194	73.64	36.82
3020	130.0	3.761	4.688	4.188	73.83	36.91
3260	127.4	3.764	4.693	4.193	74.07	37.03
300	116.5	3.753	4.681	4.185	73.52	36.76
300	120.9	3.747	4.688	4.172	73.30	36.65
300	121.5	3.743	4.686	4.179	73.30	36.65
3225	130.5	3.745	4.694	4.193	73.71	36.85
3240	130.3	3.746	4.713	4.183	73.86	36.93
300	123.5	3.738	4.690	4.177	73.22	36.61
3250	131.7	3.741	4.696	4.182	73.46	36.73
3475	138.8	3.730	4.689	4.170	72.93	36.46
3330	135.9	3.740	4.692	4.171	73.18	36.59
300	133.3	3.717	4.664	4.168	72.26	36.13
3850	145.7	3.736	4.667	4.158	72.50	36.25
300	131.5	3.721	4.660	4.160	72.14	36.07
4300	150.8	3.731	4.661	4.161	72.35	36.18
300	136.2	3.715	4.651	4.158	71.84	35.92
4170	156.6	3.723	4.663	4.134	71.77	35.89
3350	152.9	3.719	4.660	4.151	71.95	35.97
300	140.8	3.716	4.659	4.136	71.60	35.80
3835	159.0	3.712	4.659	4.139	71.58	35.79
300	144.1	3.709	4.653	4.130	71.27	35.64
3600	162.3	3.703	4.652	4.134	71.21	35.61
300	147.4	3.695	4.634	4.136	70.82	35.41
300	153.4	3.692	4.628	4.135	70.65	35.33

Table 2: Elastic parameters refined for seifertite, as well as for its 3 fictive a^3, b^3, c^3 volumes. We used the Vinet isothermal compression curves and the Mie-Grüneisen approach for modeling the effect of temperature. Θ_{D0} and γ_0 are the Debye temperature and Grüneisen parameter at ambient conditions. Some parameters were fixed following the reports of (Bolfan-Casanova et al., 2009) [1] and (Wang et al., 2012) [2].

Seifertite	Volume	a^3	b^3	c^3
V_0 [Å^3]	92.73(10)	71.0(5)	129.8(3)	92.9(5)
K_0 [GPa]	304.2(3.0)	205(9)	310(4)	291(10)
K'_0	4.59[1]	4.59[1]	4.59[1]	4.59[1]
Θ_{D0} [K]	1130[2]	1130[2]	1130[2]	1130[2]
γ_0	1.61(3)	3.01(7)	5.96(20)	2.83(10)
A	1[2]	1[2]	1[2]	1[2]
B	3[2]	3[2]	3[2]	3[2]

Table 3: Measured volume changes (ΔV/V) and calculated density changes (Δρ/ρ) across the $CaCl_2$-form to seifertite transition (Figure 5A). M-03 and H-05 stand for (Murakami et al., 2003) and (Hirose et al., 2005), respectively. The Δρ/ρ are calculated using the measured ΔV/V taking into account all possible Al substitution mechanisms in SiO_2 polymorphs. The Al^{3+} substitution can imply formation of an oxygen vacancy (O), insertion of extra-interstitial Al^{3+}(Al), or coupled Al^{3+}-H^+ substitution (H). The term "O->Al", for example, means a transition from an oxygen-deficient $CaCl_2$-form to a seifertite containing interstitial Al^{3+}. ISM: Identical substitution mechanism in both polymorphs.

	ΔV/V (%)	Δρ/ρ (%)						
		ISM	**O->Al**	**Al->O**	**O->H**	**H->O**	**Al->H**	**H->Al**
SiO_2 (M-03)	-0.60	0.60	0.60	0.60	0.60	0.60	0.60	0.60
Al-6 (This study)	-0.50	0.50	2.19	-1.16	1.56	-0.55	-0.12	1.12
MORB (H-05)	2.30	-2.30	0.23	-5.39	-1.72	-4.49	-3.23	-0.38

Figure Captions

Figure 1: Selected regions of the 2D diffraction image (upper frames) and its spectral integration (lower frame) recorded *in situ* at 120 GPa and 2500 K. Regions where major seiferte diffraction peaks occur are colored in red. The number of seifertite crystallites is insufficient for a full structural refinement using the Rietveld method. However, the diffraction peak intensities are in good agreement with the structural model of seifertite (see Figure 2).

Figure 2: The diffraction spectra are refined in two steps. We first perform a full X-ray profile refinement, using the Rietveld mode and the structural model of seifertite (upper frames). Differences between experimental and calculated peak intensities are due to (i) change with pressure and temperature of the seifertite atomic parameters; the structural model that we used corresponds to ambient P-T conditions (El Goresy et al., 2008)), and (ii) an insufficient number of crystallites in the X-ray spot. In a second step, we perform a profile refinement using the Le Bail mode (lower frames; see text). In each frame, green, upper red and lower red spectra correspond to the experimental data, fully refined profile, and seifertite contribution, respectively. We also present the major d_{hkl} indexation of the seifertite diffraction peaks (we report "several" when more than 2 seifertite diffraction peaks plot at the same 2-theta position). Left and right frames present the same experimental spectrum in 2-theta ranges of 5-10 and 10-20 degrees, respectively.

Figure 3: Examples of integrated X-ray diffraction patterns for the $CaCl_2$-structured silica phase and seifertite. These patterns were recorded (A) on ID-27 beamline at 3400 K and 121 GPa and (B) on P02.2 beamline after heating at 2500 K at 103 and 114 GPa. Small bumps on the diffraction patterns up to 2500 K are due to still incomplete transformation of the starting material. Platinum and the NaCl or KCl pressure medium are also visible. The reported pressure is based on the equation of state of Pt for the diffraction pattern recorded at high temperature before quenching.

Black crosses, green and red lines are experimental measurements, fitted background and theoretical diffraction spectra, respectively.

Figure 4: Approximate phase diagram for the SiO_2-Al_2O_3 system at 2500 K. For pure SiO_2, the phase transition is well defined at ~122 GPa (M-03; (Murakami et al., 2003)). For the mid-ocean ridge basalts used in H-05 (Hirose et al., 2005), the $CaCl_2$-form and seifertite phases were observed at 100 GPa, and 123 GPa, respectively. Concerning our samples, the rectangles represent the pressure range between our samples where $CaCl_2$-form or seifertite was synthesized. The pressure uncertainty of 3 GPa is included in the rectangle sizes. The loop diagram represented here is the widest model remaining compatible with the different data sets.

Figure 5: (A) Volumes of the two silica polymorphs measured around the transition pressure at 300 K. We also report the data sets reported for pure SiO_2 (red: (Murakami et al., 2003); black dotted line: (Andrault et al., 2003)), a MORB-type material (green: (Hirose et al., 2005)), and an Al-bearing SiO_2 glass with 4 wt% Al_2O_3 (black dotted line: (Bolfan-Casanova et al., 2009)). Closed and open symbols represent the $CaCl_2$-phase and seifertite, respectively. (B) High temperature volumes (red circles) recorded for seifertite from 100 to 162 GPa and up to 4300 K. We report the isothermal compression curves calculated at 300 K, 2000 K and 3000 K for the $CaCl_2$-form (blue dotted lines) and seifertite (dashed black lines) based on the PVT EoS refined in this study.

Figure 6: Seifertite (a, b, c) unit cell parameters recorded at 300 K (blue diamonds) and up to 4300 K (purple rectangles) for pressures from 100 to 162 GPa.

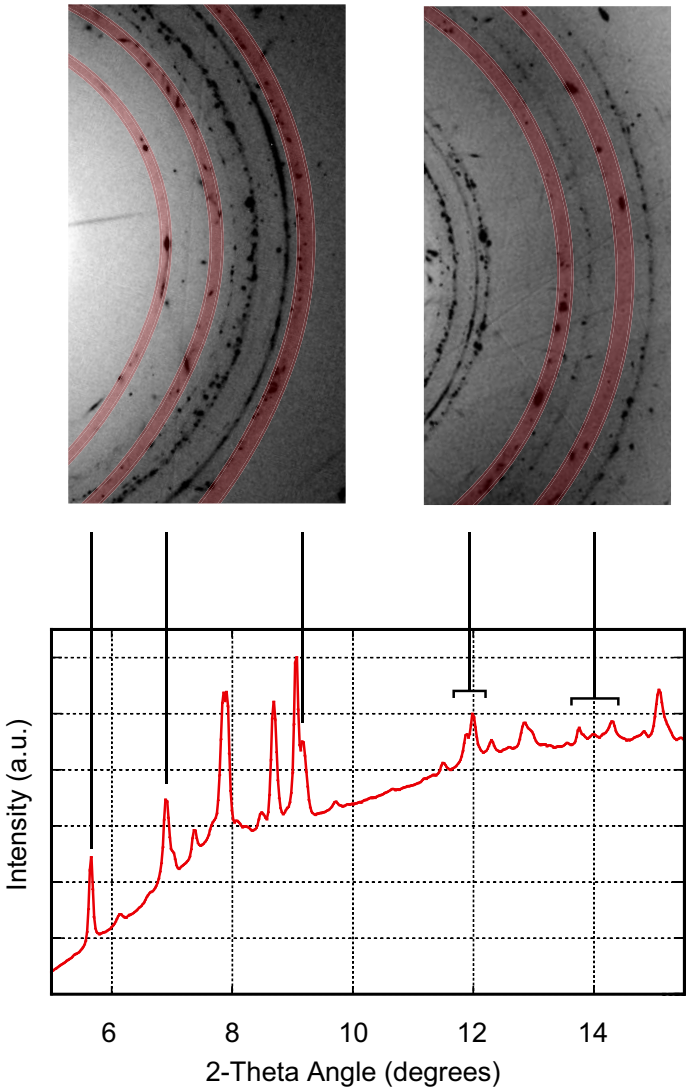

Figure 1

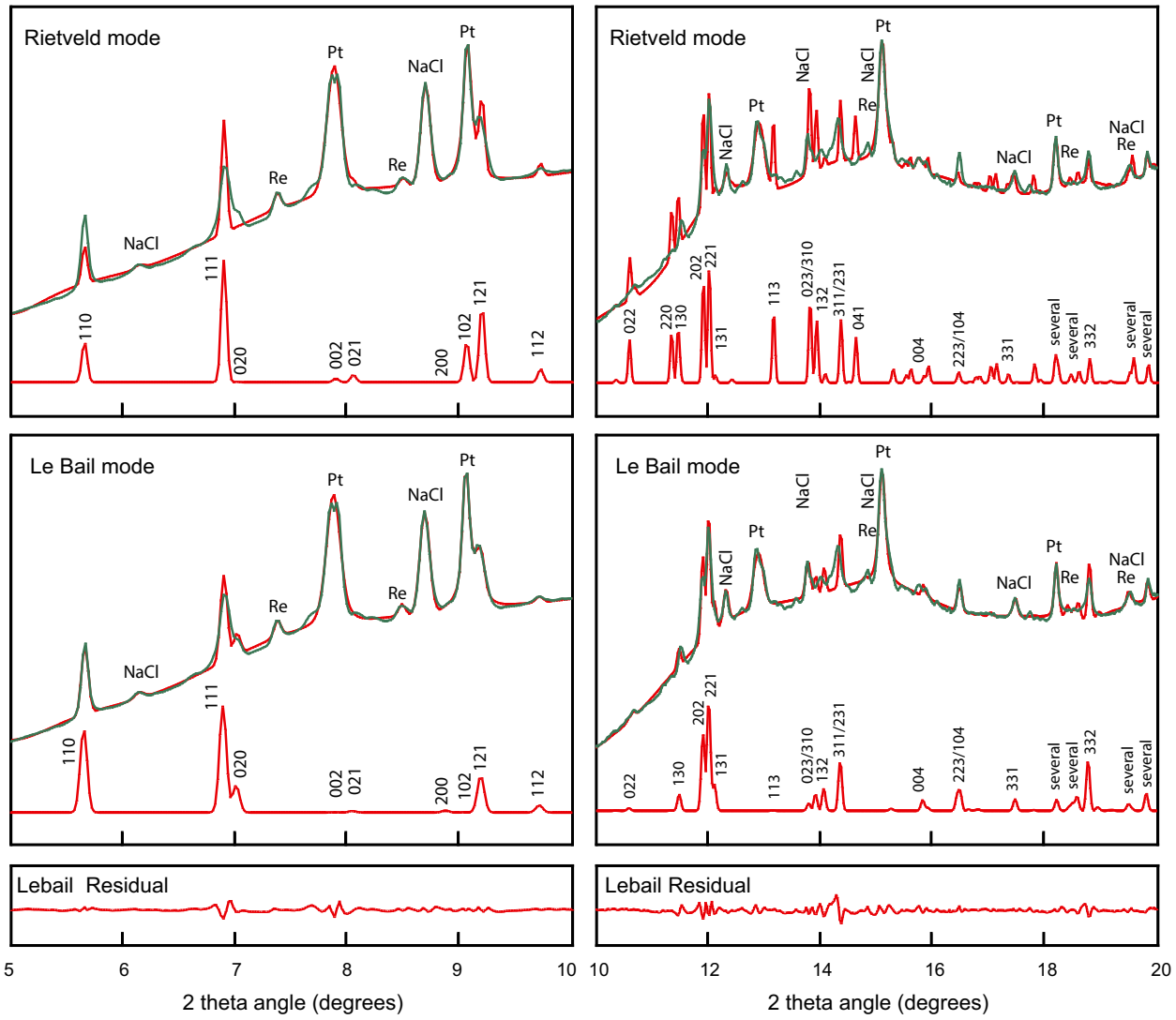
Rietveld mode
Le Bail mode
Lebail Residual
Pt
NaCl
Re
110
111
020
002
021
200
102
121
112
022
220
130
131
202
221
113
023/310
132
311/231
041
004
223/104
331
several
332
5
6
7
8
9
10
12
14
16
18
20
2 theta angle (degrees)

Figure 2

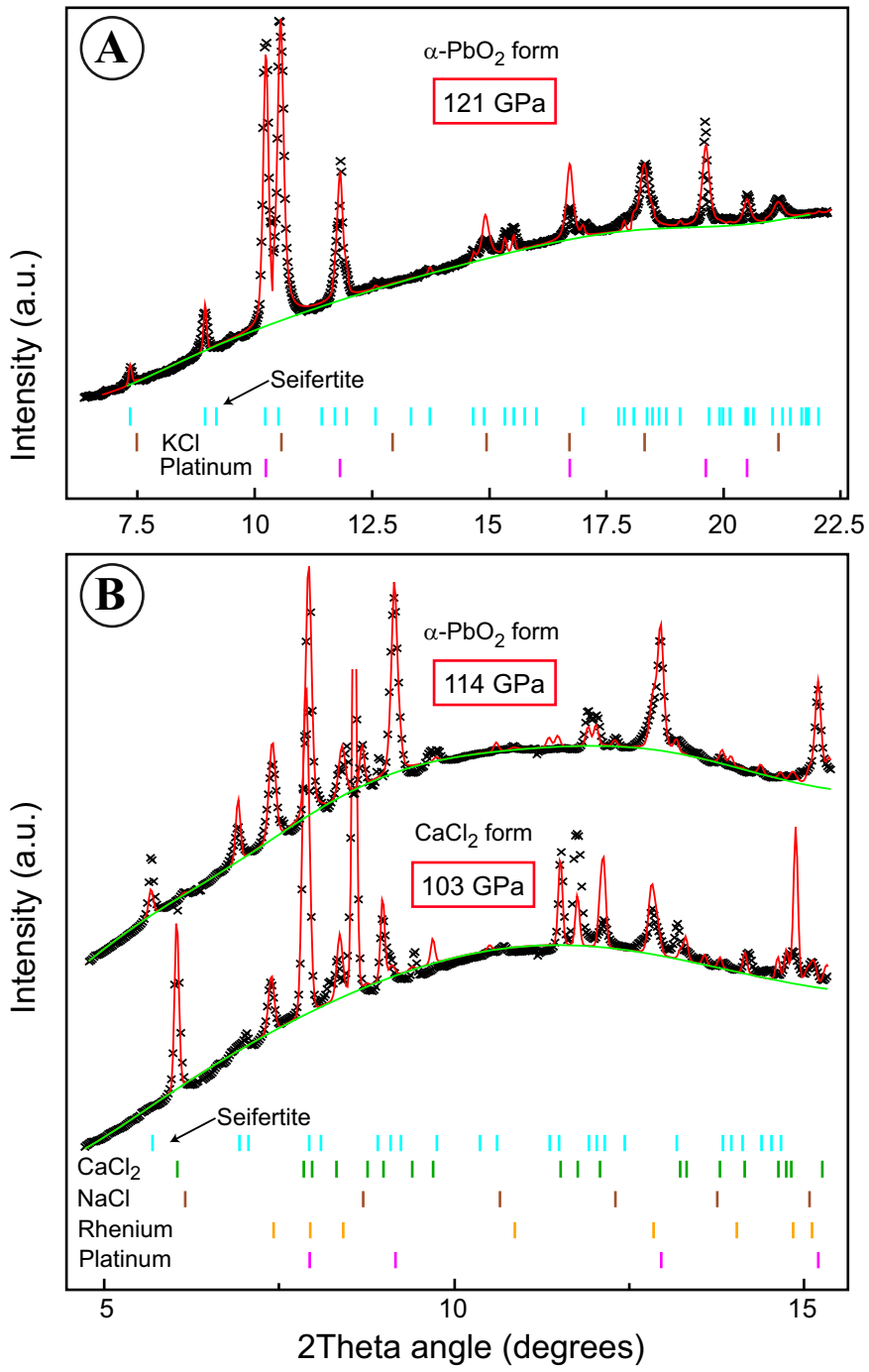
A
α-PbO2 form
121 GPa
Seifertite
KCl
Platinum
Intensity (a.u.)
7.5
10
12.5
15
17.5
20
22.5
B
α-PbO2 form
114 GPa
CaCl2 form
103 GPa
Seifertite
CaCl2
NaCl
Rhenium
Platinum
Intensity (a.u.)
5
10
15
2Theta angle (degrees)

Figure 3

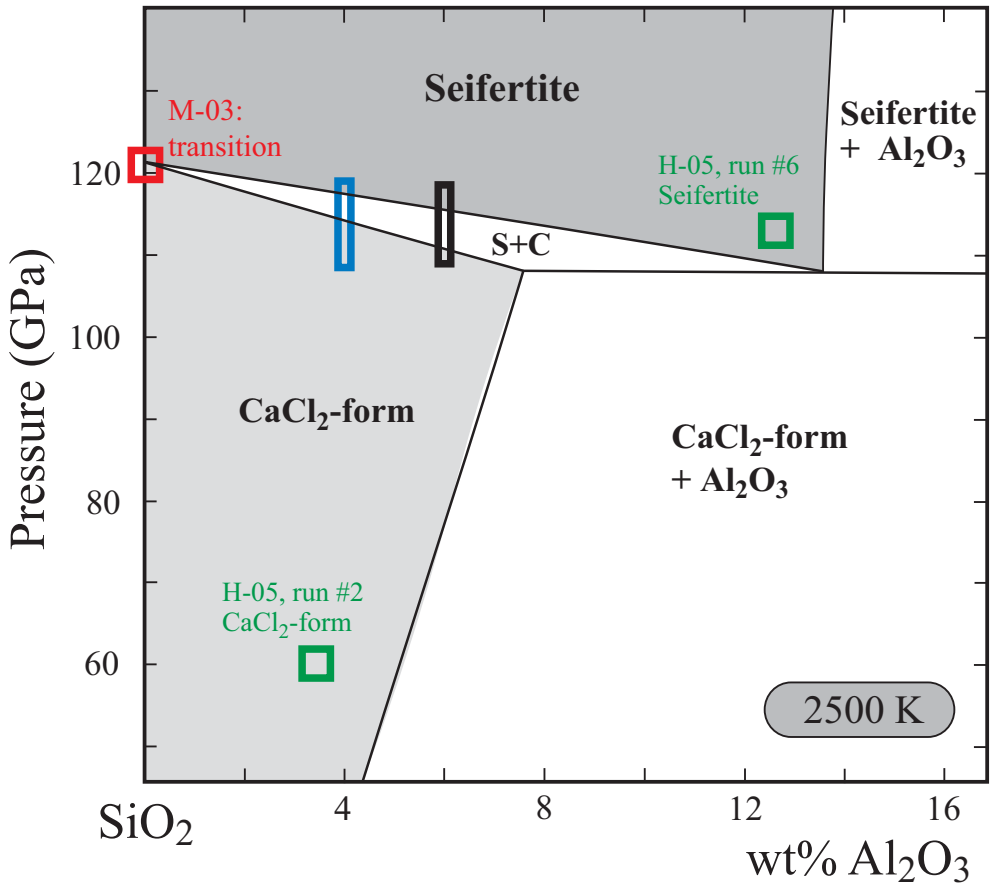
Seifertite
M-03:
transition
Seifertite
+ Al2O3
H-05, run #6
Seifertite
S+C
CaCl2-form
CaCl2-form
+ Al2O3
H-05, run #2
CaCl2-form
2500 K
Pressure (GPa)
120
100
80
60
SiO2
4
8
12
16
wt% Al2O3

Figure 4

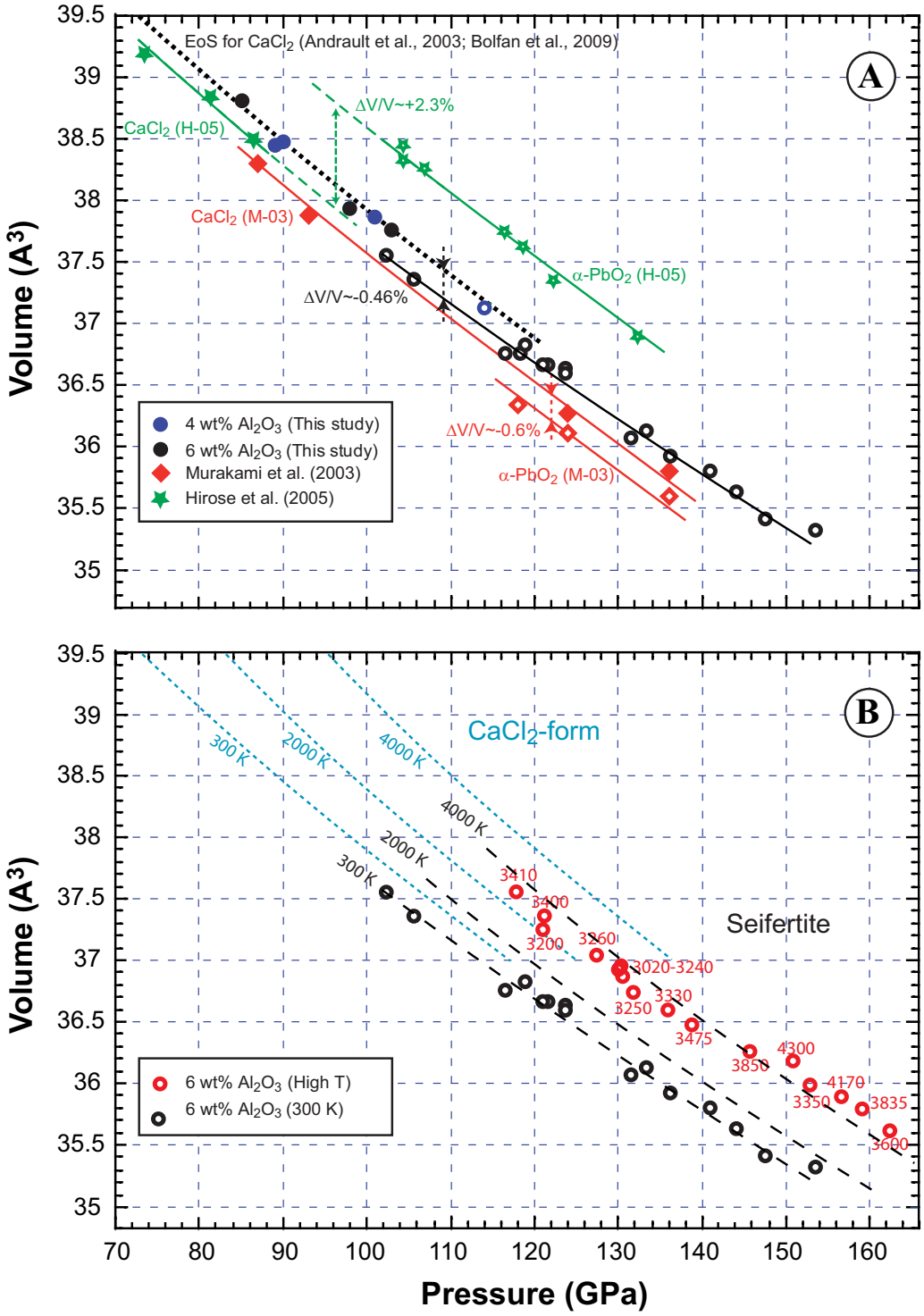
A
EoS for CaCl2 (Andrault et al., 2003; Bolfan et al., 2009)
CaCl2 (H-05)
CaCl2 (M-03)
ΔV/V~+2.3%
ΔV/V~-0.46%
ΔV/V~-0.6%
α-PbO2 (H-05)
α-PbO2 (M-03)
4 wt% Al2O3 (This study)
6 wt% Al2O3 (This study)
Murakami et al. (2003)
Hirose et al. (2005)
B
CaCl2-form
300 K
2000 K
4000 K
Seifertite
3410
3400
3200
3260
3020-3240
3330
3250
3475
4300
3850
4170
3350
3835
3600
6 wt% Al2O3 (High T)
6 wt% Al2O3 (300 K)
Volume (A3)
Pressure (GPa)

Figure 5

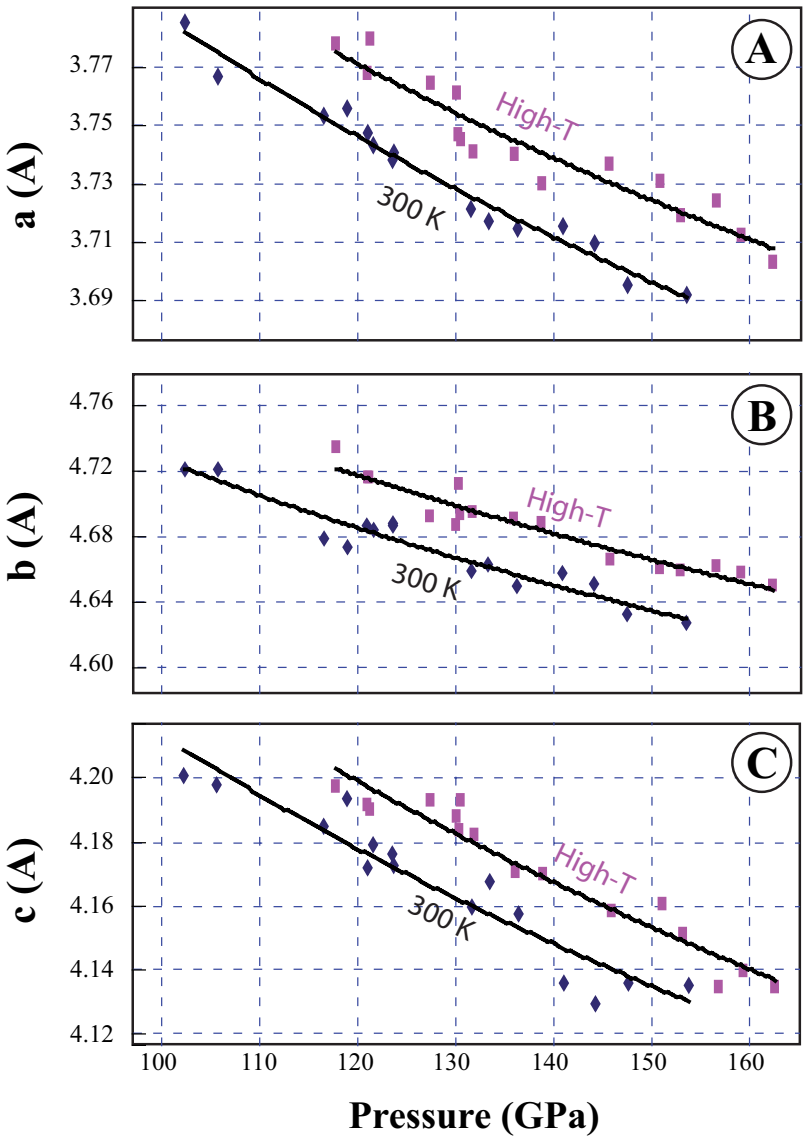
A
B
C
High-T
300 K
a (A)
b (A)
c (A)
3.77
3.75
3.73
3.71
3.69
4.76
4.72
4.68
4.64
4.60
4.20
4.18
4.16
4.14
4.12
100
110
120
130
140
150
160
Pressure (GPa)

Figure 6